Attention-Enhanced Fusion of Structural and Functional MRI for Analyzing HIV-Associated Asymptomatic Neurocognitive Impairment

Yuqi Fang[1†], Wei Wang[2†], Qianqian Wang[1], Hong-Jun Li[2*], and Mingxia Liu[1*]

[1] Department of Radiology and Biomedical Research Imaging Center, University of North Carolina at Chapel Hill, Chapel Hill, NC 27599, United States
mingxia_liu@med.unc.edu

[2] Department of Radiology, Beijing Youan Hospital, Capital Medical University, Beijing, China

[†]Equal contribution [*]Co-corresponding author

Abstract. Asymptomatic neurocognitive impairment (ANI) is a predominant form of cognitive impairment among individuals infected with human immunodeficiency virus (HIV). The current diagnostic criteria for ANI primarily rely on subjective clinical assessments, possibly leading to different interpretations among clinicians. Some recent studies leverage structural or functional MRI containing objective biomarkers for ANI analysis, offering clinicians companion diagnostic tools. However, they mainly utilize a single imaging modality, neglecting complementary information provided by structural and functional MRI. To this end, we propose an attention-enhanced structural and functional MRI fusion (ASFF) framework for HIV-associated ANI analysis. Specifically, the ASFF first extracts data-driven and human-engineered features from structural MRI, and also captures functional MRI features via a graph isomorphism network and Transformer. A *mutual cross-attention fusion module* is then designed to model the underlying relationship between structural and functional MRI. Additionally, a *semantic inter-modality constraint* is introduced to encourage consistency of multimodal features, facilitating effective feature fusion. Experimental results on 137 subjects from an HIV-associated ANI dataset with T1-weighted MRI and resting-state functional MRI show the effectiveness of our ASFF in ANI identification. Furthermore, our method can identify both modality-shared and modality-specific brain regions, which may advance our understanding of the structural and functional pathology underlying ANI.

Keywords: Multimodal fusion · HIV-associated asymptomatic neurocognitive impairment · Structural MRI · Functional MRI.

1 Introduction

Asymptomatic neurocognitive impairment (ANI) is a mild form of neurocognitive disorder observed in individuals infected with human immunodeficiency virus (HIV) [1]. While ANI patients may not show noticeable symptoms, they are

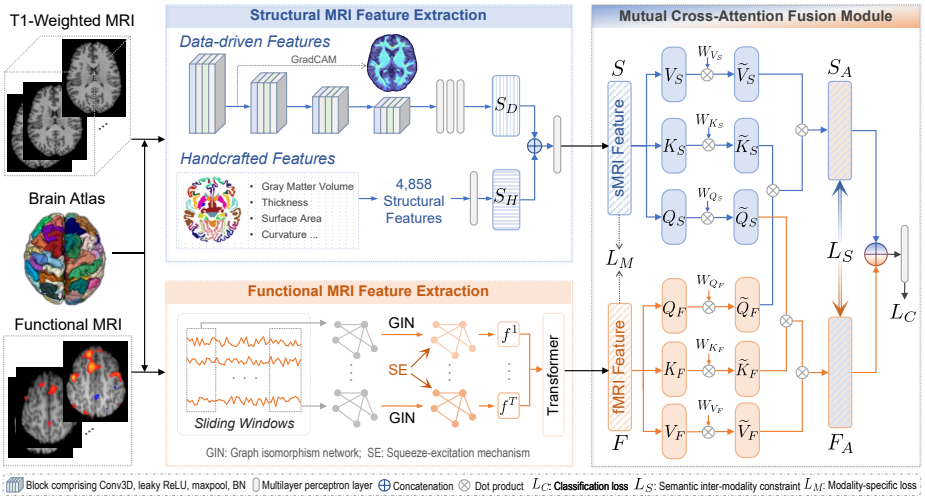

Fig. 1. Illustration of attention-enhanced structural and functional MRI fusion (ASFF) framework. It first extracts structural and functional MRI features, and then utilizes a novel *mutual cross-attention fusion module* for cross-modality relationship modeling and multimodal feature fusion. A *semantic inter-modality constraint* is also introduced to encourage consistency of multimodal features to facilitate effective feature fusion.

at risk of progressing to more severe forms of neurocognitive disorders without appropriate treatment. Therefore, early diagnosis of ANI is critical for clinicians to timely make treatment plans that can help prevent further cognitive decline. Current diagnostic criteria for ANI primarily rely on clinical assessments (*e.g.*, Frascati criteria [2]) by using a set of neurocognitive tests to evaluate an individual's cognitive functioning. But these assessment approaches exhibit a degree of subjectivity, leading to varying interpretations among clinicians [3].

To provide clinicians with objective companion diagnostic tools, some recent studies [1, 4, 5] explore the use of imaging data for ANI analysis. For instance, Kato *et al.* [4] employ T1-weighted structural MRI (T1-w sMRI) to examine ANI patients and healthy controls (HCs), and find that gray matter volume changes can serve as a clinical biomarker for ANI identification. Han *et al.* [1] use resting-state functional MRI (fMRI) to evaluate altered brain functional patterns of ANI patients, and show that brain regions in visual network exhibit a significant decrease in terms of regional homogeneity. However, these studies mainly rely on a single imaging modality (either sMRI or fMRI) for ANI analysis, neglecting complementary information offered by different modalities. Given that sMRI can provide brain anatomy and fMRI can offer brain neural activation patterns, their integration is expected to enhance the diagnostic accuracy for ANI and advance our understanding of structural and functional pathology underlying ANI.

To this end, we propose an attention-enhanced structural and functional MRI fusion (ASFF) framework for HIV-associated ANI analysis. Specifically, we first extract feature representations from sMRI and fMRI based on learning-based

methods and prior domain knowledge. We then design a *mutual cross-attention fusion module* for cross-modality relationship modeling and multimodal feature fusion. We also introduce a *semantic inter-modality constraint* to encourage consistency of multimodal features to facilitate effective feature fusion for final prediction. Experiments on an HIV-associated ANI cohort containing 137 subjects with paired sMRI and fMRI scans suggest the effectiveness of ASFF. Additionally, our method can identify modality-shared and modality-specific brain regions that may serve as imaging biomarkers for ANI analysis. To our knowledge, this is among the first attempts to investigate multimodal MRI fusion for ANI analysis.

2 Methodology

2.1 Multimodal Feature Extraction

Structural MRI Feature Extraction. Many studies [6, 7] use deep learning methods to automatically extract sMRI features. These approaches often integrate feature extraction and downstream tasks into a unified model, outputting effective task-oriented data-driven features. Other research works [8, 9] use prior domain knowledge to design handcrafted sMRI features such as cortical thickness and gray matter volume. These features are usually interpretable and could help clinicians identify potential disease-related anatomical biomarkers. In this work, we extract both data-driven and handcrafted sMRI features for ANI analysis.

As shown in Fig. 1, to extract *data-driven features*, we input T1-w sMRI into a 3D convolutional neural network that comprises 4 blocks, each containing 3D convolution operations with a kernel size of $5 \times 5 \times 5$, leaky rectified linear unit, max pooling, and batch normalization. The derived features are then vectorized and fed into 3 multilayer perceptron (MLP) layers for feature abstraction, resulting in a new feature vector $S_D \in \mathbb{R}^M$ (M=64). The choices of network architecture and hyperparameters are based on empirical experience. To extract *handcrafted features*, we follow the processing stream provided by FreeSurfer [10], resulting in 4,858 features for each sMRI scan (*e.g.*, surface area, gray matter volume, cortical thickness, curvature, and cortical gyrification). These features are then fed into an MLP to produce $S_H \in \mathbb{R}^M$. We then feed data-driven and handcrafted features $[S_D, S_H]$ into an MLP, resulting in an sMRI feature vector $S \in \mathbb{R}^M$.

Functional MRI Feature Extraction. Extracting fMRI features for studying ANI is important, which allows clinicians to characterize brain activity changes and find potential therapeutic targets. In this work, we explore fMRI features from both spatial and temporal aspects, since brain regions are interconnected spatially and also exhibit functional changes over time.

Specifically, we first parcellate the brain into N regions-of-interest (ROIs) based on the AAL atlas and use the sliding window technique to partition fMRI time series into T segments to model brain functional variability. We then represent fMRI data at each window as a graph, where each node denotes a brain ROI and each edge denotes Pearson's correlation between paired ROIs [11]. To

capture *spatial fMRI features* across the entire brain, we employ an established graph isomorphism network (GIN) [12] to update the representation of each ROI by aggregating features from its neighbors. We also embed squeeze-excitation (SE) [13] in each ROI to identify their unique contribution to the downstream task. By averaging the representations of all ROIs, we obtain spatial fMRI feature f^t (t=1, $\cdots$, T) for the t-th sliding window. With these spatial features, we then learn *temporal fMRI features* across different windows to examine dynamic changes in brain activity. To achieve that, we employ a Transformer [14] to model attention across windows, resulting in a spatiotemporal fMRI feature $F \in \mathbb{R}^M$. The rationale behind this lies in the Transformer's ability to capture long-range dependencies in sequential data. Here, given that neural activity captured by fMRI evolves over time, Transformer excels at capturing the dependencies across multiple windows by processing the entire fMRI sequence simultaneously.

2.2 Mutual Cross-Attention Fusion

Given that sMRI and fMRI provide complementary information, their integration is expected to improve diagnostic performance. Recent studies suggest that alterations in brain structure may influence functional changes [15], and vice versa [16]. Intuitively, modeling mutual relationship between sMRI and fMRI is useful to advance our understanding of brain neuroplasticity underlying ANI. Accordingly, we design a *mutual cross-attention fusion module* to capture intrinsic relationships between sMRI and fMRI, followed by feature fusion for prediction.

To capture mutual cross-attention, we generate three new vectors based on the sMRI feature S: query Q_S, key K_S, and value V_S (Q_S=K_S=V_S=S). We then derive $\widetilde{Q}_S$, $\widetilde{K}_S$, and $\widetilde{V}_S$ using learnable weight matrices W_{Q_S}, W_{K_S}, and W_{V_S}:

$$\widetilde{Q}_S = Q_S \otimes W_{Q_S}, \quad \widetilde{K}_S = K_S \otimes W_{K_S}, \quad \widetilde{V}_S = V_S \otimes W_{V_S}, \tag{1}$$

where $\otimes$ represents dot product, $\widetilde{Q}_S$ serves as structural context to the fMRI modality, $\widetilde{K}_S$ represents sMRI features intended for matching with fMRI, and $\widetilde{V}_S$ corresponds to structural representations used for computing attended sMRI features. Similarly, we derive $\widetilde{Q}_F$, $\widetilde{K}_F$, and $\widetilde{V}_F$ based on the fMRI feature F. To model relationships between sMRI and fMRI, we capture their mutual relevance and result in two attended sMRI and fMRI features as follows:

$$S_A = softmax(\widetilde{Q}_F \otimes \widetilde{K}_S / \sqrt{M}) \otimes \widetilde{V}_S, \tag{2}$$

$$F_A = softmax(\widetilde{Q}_S \otimes \widetilde{K}_F / \sqrt{M}) \otimes \widetilde{V}_F, \tag{3}$$

where $\widetilde{Q}_F \otimes \widetilde{K}_S$ in S_A captures the relevance between fMRI-related query $\widetilde{Q}_F$ and sMRI-related key $\widetilde{K}_S$, which is then scaled by feature dimension M for computation stability and fed into a softmax function to produce an attention score. By multiplying this attention score with $\widetilde{V}_S$, we can highlight sMRI features that are more relevant to fMRI. Similarly, F_A emphasizes fMRI features that are more relevant to sMRI. After obtaining S_A and F_A, we concatenate them and feed them into an MLP for final prediction.

2.3 Semantic Inter-Modality Constraint

To further model underlying dependencies of sMRI and fMRI, we design a semantic inter-modality constraint L_S to encourage consistency of S_A and F_A:

$$L_S = -\sum_{i=1}^{B} g_i \cdot log(S_A \otimes F_A) + g_i \cdot log(F_A \otimes S_A), \tag{4}$$

where B denotes the number of subjects in one training batch, and $S_A \otimes F_A \in \mathbb{R}^{B\times B}$ is a matrix with its (m,n)-th entry measuring the similarity between sMRI of m-th subject and fMRI of n-th subject. Each diagonal value of $S_A \otimes F_A$ measures feature consistency of the same subject while the off-diagonal elements evaluate consistency across different subjects. The term $g_i \in \mathbb{R}^B$ is a one-hot label vector corresponding to i-th subject, where its i-th entry is set to 1 while all other entries are 0. By optimizing $g_i \cdot log(S_A \otimes F_A)$, we aim to focus on diagonal values of $S_A \otimes F_A$. In this way, we explicitly encourage multimodal semantic features (*i.e.*, S_A and F_A) of the same subject to be close, and implicitly place those of distinct subjects further apart. The second term of Eq. (4) follows the same principle, where (m,n)-th entry of $F_A \otimes S_A$ evaluates the semantic similarity between fMRI of m-th subject and sMRI of n-th subject. And optimizing $g_i \cdot log(F_A \otimes S_A)$ also enforces multimodal feature consistency of the same subject.

Objective Function. Besides L_S, we introduce two additional losses for model training, *i.e.*, a classification loss L_C and a modality-specific loss L_M. As illustrated in Fig. 1, L_C is designed based on concatenated features $[S_A,F_A]$, formulated as:

$$L_C = -\sum_{i=1}^{B} y_i log(p_i) + (1-y_i) log(1-p_i), \tag{5}$$

where p_i indicates the probability derived from the concatenated features of i-th subject followed by an MLP; $y_i \in \{1,0\}$ is the ground-truth label (*e.g.*, 1 for ANI, 0 for HC). Considering that each single modality can also provide useful information, we use sMRI and fMRI features to produce prediction separately, with the loss L_M defined as:

$$L_M = -\sum_{i=1}^{B} (y_i log(p_{S_i}) + (1-y_i) log(1-p_{S_i})) - \sum_{i=1}^{B} (y_i log(p_{F_i}) + (1-y_i) log(1-p_{F_i})), \tag{6}$$

where p_{S_i} and p_{F_i} denote the probabilities derived from sMRI and fMRI features (*i.e.*, S and F) of the i-th subject, respectively. The final objective function is formulated as: $L = L_C + L_S + L_M$. Our ASFF is trained end-to-end via PyTorch. The Adam is used for model optimization, and batch size is 4. The initial learning rate is set to 0.0001 and dropped by 0.5 every 50 epochs, and the training epoch is empirically set as 150.

3 Experiment and Discussion

Materials and Image Preprocessing. A dataset from a local hospital (named **ANID**) is used in the experiments. It contains 68 HIV-associated ANI patients and 69 HCs, each with paired T1-w sMRI and resting-state fMRI scans. The demographics of the studied subjects are given in *Supplementary Materials*. All sMRI data are preprocessed using a standard pipeline with FreeSurfer [10], including bias field correction, motion correction, intensity normalization, registration to Montreal Neurological Institute (MNI) space, and skull stripping. All fMRI data are preprocessed using

Table 1. Results (%) of ASFF and nine competing methods on ANID dataset.

Method	AUC	ACC	F1	SEN	SPE	PRE
SVM [18]	55.65±3.96	54.76±5.43	54.92±5.49	55.24±6.46	54.29±7.13	54.8±5.32
RF [19]	53.99±10.16	53.33±9.11	46.49±12.61	42.86±17.56	63.81±13.67	54.56±10.21
ResNet [20]	56.80±9.65	55.71±7.16	52.85±6.75	49.52±6.46	61.90±11.66	57.17±8.76
GCN [21]	63.53±8.88	57.70±8.24	58.07±6.54	60.85±15.91	57.59±17.07	59.31±13.04
GAT [22]	65.80±13.10	57.70±13.33	59.81±9.22	63.77±15.52	56.46±28.89	61.65±19.88
TFM [14]	56.35±7.88	55.24±7.74	58.03±11.74	**64.76±18.22**	45.71±9.81	53.49±7.34
LSTM [23]	54.51±3.70	52.38±2.13	44.88±12.20	44.76±28.03	60.00±28.03	53.67±4.12
PAD [24]	64.08±4.68	60.00±4.10	59.63±3.78	59.05±3.81	60.95±5.55	60.30±4.29
CMCA [25]	67.14±4.91	60.50±4.00	58.70±2.24	53.33±3.56	68.42±11.04	66.22±7.53
ASFF (Ours)	**68.66±5.73**	**65.24±4.90**	**63.98±4.85**	61.91±6.73	**68.57±9.33**	**66.86±6.25**

DPARSF [17], with the following steps: discarding the first 10 volumes, slice timing correction, head motion correction, bandpass filtering (0.01-0.10 Hz), nuisance signal removal, spatial normalization to MNI space, and brain partition into $N = 116$ ROIs based on AAL atlas. The regional mean fMRI time series are extracted for each subject.

Competing Methods. We compare the proposed ASFF with nine competing approaches using the ANID dataset for ANI vs. HC classification, including 1) **SVM** [18] and 2) **RF** [19] that feed 4,858 handcrafted sMRI features into an SVM and random forest model, respectively; 3) **ResNet** [20] that inputs sMRIs to a 3D ResNet; 4) **GCN** [21] and 5) **GAT** [22] that capture fMRI features using a graph convolutional network and graph attention network, respectively; 6) **TFM** [14] that utilizes a Transformer to model fMRI dynamics; 7) **LSTM** [23] that captures long-term dependencies for fMRI timeseries; 8) **PAD** [24] that uses XGBoost as the classifier with concatenated handcrafted sMRI and fMRI features as input; and 9) **CMCA** [25] that employs a graph neural network with sMRI and fMRI features as node features. For all methods, we randomly split the dataset into training and test sets with a ratio of 70/30. This process is repeated five times, and the averaged results are recorded. Six metrics are used for evaluation, including area under the ROC curve (AUC), accuracy (ACC), F1-score (F1), sensitivity (SEN), specificity (SPE), and precision (PRE).

Classification Results. The mean and standard deviation results of ten different methods for ANI diagnosis are reported in Table 1. From Table 1, we can see that the methods using both sMRI and fMRI (*i.e.*, PAD, CMCA, and ASFF) outperform the methods that use one single modality in most cases. This implies that multimodal fusion can enhance diagnostic accuracy by leveraging complementary information from different modalities. Moreover, our ASFF shows superior prediction results compared with the other two multimodal approaches (*i.e.*, PAD and CMCA). For instance, the ASFF achieves improved AUC scores of 4.58% and 1.52% compared to PAD and CMCA, respectively. The possible reason may be that the ASFF can capture the inherent relationships across the two modalities, while the PAD and CMCA only concatenate multimodal features without considering intrinsic relevance between sMRI and fMRI, thus leading to suboptimal performance.

Ablation Study. We compare the ASFF with its three variants: 1) **ASFFw/oA** that removes the mutual cross-attention fusion module, *i.e.*, sMRI features S and fMRI features F are directly concatenated for prediction; 2) **ASFFw/oS** and 3) **ASFFw/oM**

Table 2. Results (%) of the ASFF and its three variants on ANID dataset.

Method	AUC (%)	ACC (%)	F1 (%)	SEN (%)	SPE (%)	PRE (%)
ASFFw/oA	62.95±9.09	60.48±6.67	56.64±6.37	51.43±5.55	**69.52±10.69**	63.57±9.38
ASFFw/oS	64.04±6.30	60.95±6.32	58.79±3.31	55.24±4.86	66.67±16.22	64.72±11.15
ASFFw/oM	61.95±6.26	59.05±3.50	55.08±3.89	50.48±6.46	67.62±9.23	61.50±5.32
ASFF (Ours)	**68.66±5.73**	**65.24±4.90**	**63.98±4.85**	**61.91±6.73**	68.57±9.33	**66.86±6.25**

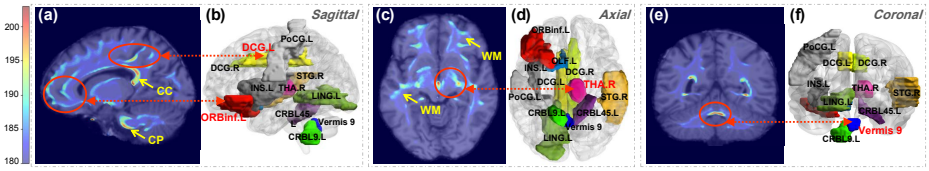

Fig. 2. Illustration of ANI-associated brain regions derived from sMRI (a, c, e) and fMRI (b, d, f) in three views. CC: corpus callosum; WM: white matter; CP: cerebellar peduncle. The full names of brain regions are listed in *Supplementary Materials.*

that train ASFF without considering the semantic inter-modality constraint L_S and the modality-specific loss L_M, respectively. The results of ASFF and its variants are listed in Table 2. From Table 2, we can see that ASFF outperforms ASFFw/oA in most cases, implying that capturing the underlying relationships between sMRI and fMRI is beneficial to final prediction. The possible reason may be that brain structure and function can influence each other in a bidirectional way, and there may exist inherent relationships between sMRI and fMRI modalities. Thus, the mutual cross-attention proposed in our ASFF could model such relationships by enforcing feature relevance across both modalities, leading to improved diagnostic performance. *In addition*, we find that ASFF generally shows superior results to ASFFw/oS and ASFFw/oM, which indicates the importance of introducing L_S and L_M in ANI identification. The L_S encourages consistent features across sMRI and fMRI, while L_M helps add modality-specific information to ASFF. By using these two losses, it is expected that both modality-shared and modality-specific features can be captured, as proven in the following subsection.

Discriminative Brain Regions. In Fig. 2, we visualize the discriminative brain regions identified by our method from sMRI and fMRI. Specifically, for sMRI, we generate attention maps related to ANI identification using GradCAM [26] based on all ANI patients correctly classified by our ASFF, as shown in Fig. 2 (a, c, e). For fMRI, we employ squeeze-excitation [13] to identify the contributions of each brain ROI to final diagnosis, and the top 10% informative ROIs are shown in Fig. 2 (b, d, f). By comparing the discriminative brain regions across sMRI and fMRI, we find the following **modality-shared** regions, *i.e.*, *prefrontal cortex*, *cingulate*, *thalamus*, and *cerebellar vermis*, which are outlined by red circles and arrows in the figure. Specifically, the *prefrontal cortex* is highly involved in many higher-order cognitive functions, such as working memory and decision making [27], and its abnormality could cause neurocognitive impairment in ANI patients [28]. The *cingulate* has also been shown related to cognitive process [29]. And ANI patients may exhibit disrupted neural circuits involving this region, leading to structural and functional aberration [30]. In terms of *thalamus*, some existing studies report that this region shows reduced volume [31] and decreased functional connectivity within thalamic prefrontal circuit [30] in HIV-positive patients. These aberrant changes may play a significant role in cognitive dysfunction in ANI. In

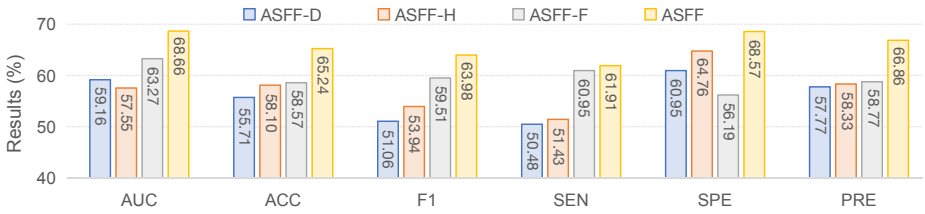

Fig. 3. Results of influence of different imaging modalities on ANI diagnosis.

addition, the *cerebellar vermis* plays an important part in spinocerebellar pathway [32]. Even ANI patients are in the early stage of cognitive impairment without obvious clinical symptoms, we still find anatomical and functional changes in this region, which can serve as a potential indicator for assessing disease-related progression.

Moreover, our ASFF identifies some **modality-specific** brain regions contributing to diagnosis. (1) From structural MRI, we find that *white matter* (WM) exhibits severe abnormality in ANI patients, consistent with many studies [33,34]. The pattern of white matter changes may reflect regionally specific HIV neuropathological process [35]. We also find *corpus callosum* (CC) and *cerebellar peduncle* (CP) play important roles in ANI diagnosis, which are in line with [36]. The underlying reason may be that both CC and CP are close to cerebrospinal fluid (CSF) and choroid plexus, while HIV-infected patients may have CSF viral escape and the choroid plexus has been shown to be rich in HIV virus particles [37]. (2) From functional MRI, we find that *insula* [1], *olfactory* [38], *lingual gyrus* [4], and *superior temporal gyrus* [5] are associated with ANI. These findings indicate that the altered functional connectivities of these regions contribute to cognitive dysfunction in ANI patients, which could be used as potential fMRI biomarkers to improve ANI diagnosis in clinical practice.

Influence of Imaging Modalities. To investigate the influence of each modality on ANI diagnosis, we compare the proposed ASFF with its three variants: 1) **ASFF-D** and 2) **ASFF-H** that use data-driven and handcrafted sMRI features for prediction, respectively, where their model architectures are the same as that used in ASFF; and 3) **ASFF-F** that employs the same GIN and Transformer as ASFF to extract fMRI features for end-to-end prediction, without using structural MRI. The results of these three variants and ASFF are reported in Fig. 3. From Fig. 3, we can see that our ASFF that integrates both modalities outperforms the other methods that use only one single modality, suggesting the necessity of sMRI and fMRI fusion. Moreover, an interesting observation is that ASFF-F generally yields superior results compared to ASFF-D and ASFF-H. This implies that functional MRI may help identify early brain alterations and abnormalities in ANI before they are detectable from structural MRI.

4 Conclusion and Future Work

This paper designs an attention-enhanced structural and functional MRI fusion (ASFF) framework for HIV-associated ANI diagnosis. The ASFF captures informative features from structural and functional MRI, and then introduces a mutual cross-attention fusion module to model the underlying relationship between two modalities. A semantic

inter-modality constraint is also proposed to further facilitate multimodal feature fusion. The experiments show the effectiveness of our method. In addition, our method helps identify both modality-shared and modality-specific brain regions underlying ANI, which could be employed as potential imaging biomarkers for early diagnosis.

In the current study, we only have a limited number of studied subjects. In future work, we are planning to collect more data and also generalize a foundation model pretrained on large-scale public datasets to our ASFF for improved diagnosis. Additionally, we only utilize two modalities (*i.e.*, T1-weighted sMRI and resting-state fMRI) in this work. It is interesting to incorporate other modalities such as diffusion MRI to boost multi-modality data fusion and automated detection of ANI.

Acknowledgments. Y. Fang and M. Liu were supported in part by NIH grant RF1AG073297. W. Wang was supported by the Beijing Youan Hospital Intramural Project for the Incubation of Young and Middle-aged Talent (No. BJYAYY-YN2023-04) and Beijing Hospital Authority Clinical Medicine Development Special Funding (No. ZLRK202333).

Disclosure of Interests. The authors have no competing interests to declare that are relevant to the content of this article.

References

1. Han, S., Aili, X., Ma, J., Liu, J., et al.: Altered regional homogeneity and functional connectivity of brain activity in young HIV-infected patients with asymptomatic neurocognitive impairment. Frontiers in Neurology **13** (2022) 982520
2. Wei, J., Hou, J., Su, B., Jiang, T., Guo, C., Wang, W., Zhang, Y., Chang, B., Wu, H., Zhang, T.: The prevalence of frascati-criteria-based HIV-associated neurocognitive disorder (HAND) in HIV-infected adults: A systematic review and meta-analysis. Frontiers in Neurology **11** (2020) 581346
3. Gandhi, N.S., Skolasky, R.L., Peters, K.B., Moxley, R.T., Creighton, J., Roosa, H.V., et al.: A comparison of performance-based measures of function in HIV-associated neurocognitive disorders. Journal of NeuroVirology **17** (2011) 159–165
4. Kato, T., Yoshihara, Y., Watanabe, D., Fukumoto, M., Wada, K., Nakakura, T., Kuriyama, K., et al.: Neurocognitive impairment and gray matter volume reduction in HIV-infected patients. Journal of NeuroVirology **26** (2020) 590–601
5. Zhao, J., Wu, Y., Chen, F., Zhao, H., Chen, J., Jing, B., Li, H.: Distance-specific functional connectivity strength alterations in human immunodeficiency virus asymptomatic neurocognitive impairment patients: A cross-sectional study. Quantitative Imaging in Medicine and Surgery **14**(2) (2024) 1835843–1831843
6. Abrol, A., Fu, Z., Salman, M., Silva, R., Du, Y., Plis, S., Calhoun, V.: Deep learning encodes robust discriminative neuroimaging representations to outperform standard machine learning. Nature Communications **12**(1) (2021) 353
7. Billot, B., et al.: SynthSeg: Segmentation of brain MRI scans of any contrast and resolution without retraining. Medical Image Analysis **86** (2023) 102789
8. Madre, M., Canales-Rodríguez, E.J., et al.: Structural abnormality in schizophrenia versus bipolar disorder: A whole brain cortical thickness, surface area, volume and gyrification analyses. NeuroImage: Clinical **25** (2020) 102131
9. Wang, Y., Leiberg, K., Ludwig, T., Little, B., Necus, J.H., et al.: Independent components of human brain morphology. NeuroImage **226** (2021) 117546

10. Fischl, B.: FreeSurfer. NeuroImage **62**(2) (2012) 774–781
11. Kim, B.H., Ye, J.C., Kim, J.J.: Learning dynamic graph representation of brain connectome with spatio-temporal attention. Advances in Neural Information Processing Systems **34** (2021) 4314–4327
12. Xu, K., Hu, W., Leskovec, J., Jegelka, S.: How powerful are graph neural networks? In: International Conference on Learning Representations. (2019)
13. Hu, J., Shen, L., Sun, G.: Squeeze-and-Excitation networks. In: Proceedings of the IEEE Conference on Computer Vision and Pattern Recognition. (2018) 7132–7141
14. Vaswani, A., Shazeer, N., Parmar, N., Uszkoreit, J., Jones, L., et al.: Attention is all you need. Advances in Neural Information Processing Systems **30** (2017)
15. Brosch, K., Stein, F., Schmitt, S., et al.: Reduced hippocampal gray matter volume is a common feature of patients with major depression, bipolar disorder, and schizophrenia spectrum disorders. Molecular Psychiatry **27**(10) (2022) 4234–4243
16. Nenning, K.H., Furtner, J., Kiesel, B., Schwartz, E., Roetzer, T., Fortelny, N., Bock, C., Grisold, A., Marko, M., et al.: Distributed changes of the functional connectome in patients with glioblastoma. Scientific Reports **10**(1) (2020) 18312
17. Yan, C., Zang, Y.: DPARSF: A matlab toolbox for "pipeline" data analysis of resting-state fMRI. Frontiers in Systems Neuroscience **4** (2010) 1377
18. Steinwart, I., Christmann, A.: Support vector machines. Springer Science & Business Media (2008)
19. Breiman, L.: Random forests. Machine Learning **45** (2001) 5–32
20. He, K., et al.: Deep residual learning for image recognition. In: Proceedings of the IEEE Conference on Computer Vision and Pattern Recognition. (2016) 770–778
21. Kipf, T.N., Welling, M.: Semi-supervised classification with graph convolutional networks. arXiv preprint arXiv:1609.02907 (2016)
22. Velickovic, P., Cucurull, G., Casanova, A., Romero, A., Lio, P., Bengio, Y., et al.: Graph attention networks. Stat **1050**(20) (2017) 10–48550
23. Hochreiter, S., Schmidhuber, J.: Long short-term memory. Neural Computation **9** (1997) 1735–1780
24. Dekhil, O., Ali, M., El-Nakieb, Y., Shalaby, A., Soliman, A., Switala, A., Mahmoud, A., et al.: A personalized autism diagnosis CAD system using a fusion of structural MRI and resting-state functional MRI data. Frontiers in Psychiatry **10** (2019) 392
25. Chen, X., Ke, P., Huang, Y., Zhou, J., et al.: Discriminative analysis of schizophrenia patients using graph convolutional networks: A combined multimodal MRI and connectomics analysis. Frontiers in Neuroscience **17** (2023) 1140801
26. Selvaraju, R.R., Cogswell, M., Das, A., Vedantam, R., et al.: Grad-CAM: Visual explanations from deep networks via gradient-based localization. In: Proceedings of the IEEE International Conference on Computer Vision. (2017) 618–626
27. Frith, C., Dolan, R.: The role of the prefrontal cortex in higher cognitive functions. Cognitive Brain Research **5**(1-2) (1996) 175–181
28. Lew, B.J., McDermott, T.J., Wiesman, A.I., O'Neill, J., Mills, M.S., Robertson, K.R., Fox, H.S., Swindells, S., et al.: Neural dynamics of selective attention deficits in HIV-associated neurocognitive disorder. Neurology **91** (2018) e1860 – e1869
29. Bush, G., Luu, P., Posner, M.I.: Cognitive and emotional influences in anterior cingulate cortex. Trends in Cognitive Sciences **4**(6) (2000) 215–222
30. Liu, D., Zhao, C., Wang, W., Wang, Y., Li, R., Sun, J., Liu, J., Liu, M., Zhang, X., et al.: Altered gray matter volume and functional connectivity in human immunodeficiency virus-infected adults. Frontiers in Neuroscience **14** (2020) 601063
31. Nichols, M.J., Gates, T.M., Soares, J.R., Moffat, K.J., Rae, C.D., Brew, B.J., Cysique, L.A.: Atrophic brain signatures of mild forms of neurocognitive impairment in virally suppressed HIV infection. AIDS **33**(1) (2019) 55–66

32. Coffman, K.A., Dum, R.P., Strick, P.L.: Cerebellar vermis is a target of projections from the motor areas in the cerebral cortex. Proceedings of the National Academy of Sciences **108**(38) (2011) 16068–16073
33. Alakkas, A., Ellis, R.J., et al.: White matter damage, neuroinflammation, and neuronal integrity in hand. Journal of Neurovirology **25** (2019) 32–41
34. Clifford, D.B., Ances, B.M.: HIV-associated neurocognitive disorder. The Lancet Infectious Diseases **13**(11) (2013) 976–986
35. Gongvatana, A., Cohen, R.A., et al.: Clinical contributors to cerebral white matter integrity in HIV-infected individuals. Journal of Neurovirology **17** (2011) 477–486
36. Qi, Y., Wang, W., Rao, B., Yang, X., et al.: Value of radiomic analysis combined with diffusion tensor imaging in early diagnosis of HIV-associated neurocognitive disorders. Journal of Magnetic Resonance Imaging **58** (2023) 1882–1891
37. Petito, C.K., Chen, H., et al.: HIV infection of choroid plexus in AIDS and asymptomatic HIV-infected patients suggests that the choroid plexus may be a reservoir of productive infection. Journal of Neurovirology **5**(6) (1999) 670–677
38. Hornung, D.E., Kurtz, D.B., Bradshaw, C.B., et al.: The olfactory loss that accompanies an HIV infection. Physiology & Behavior **64**(4) (1998) 549–556